Thermal conductivity of group-III phosphides: The special case of GaP

Bonny Dongre,[1] Jesús Carrete,[1] Natalio Mingo,[2] and Georg K. H. Madsen[1,*]
[1]*Institute of Materials Chemistry, TU Wien, A-1060 Vienna, Austria*
[2]*Université Grenoble-Alpes, CEA, LITEN, 17 rue des Martyrs, F-38054 Grenoble, France*

(Received 5 August 2022; revised 3 November 2022; accepted 8 November 2022; published 14 November 2022)

We calculate the lattice thermal conductivity of cubic group-III phosphides by solving the linearized Boltzmann transport equation for phonons and discuss how there is a large disagreement between the literature values for GaP. We find the presence of comparably large third-order interatomic force constants at large interaction distances that influence the thermal conductivity of GaP. When both four-phonon scattering and the contributions from the long-range interactions are included in the calculation, a thermal conductivity of 76 $\mathrm{W\,m^{-1}\,K^{-1}}$ is obtained at room temperature, in good agreement with a reported experimental value of 77 $\mathrm{W\,m^{-1}\,K^{-1}}$. Our results show the importance of carrying out convergence tests with respect to all the calculation parameters and could help explain the thermal conductivity in other systems where similar ambiguities are found.

DOI: 10.1103/PhysRevB.106.205202

I. INTRODUCTION

The high lattice thermal conductivity (κ_ℓ) of group-III phosphides plays a vital role in technologies as varied as optoelectronics, photovoltaics, and phononics [1,2]. A successful approach to the prediction of κ_ℓ has been a combination of second- and third-order interatomic force constants (IFCs) calculated with density functional theory (DFT) and the linearized Boltzmann transport equation (BTE) [3]. The method generally shows good agreement with experiments, especially for this type of structure with a high thermal conductivity [4]. In principle, it is also parameter free, but in practice minute attention has to be paid to the underlying computational parameters.

Several studies have considered the calculation of κ_ℓ for the group-III phosphides [5–9] and, as expected for this type of calculation, both a good internal concordance and a good agreement with the experimental values is generally found. However, the results for GaP stand out. As shown in Table I, there is a large spread in κ_ℓ calculated considering only three-phonon (3ph) scattering, with the lowest value being 103 and highest 157 $\mathrm{W\,m^{-1}\,K^{-1}}$. Generally, the theoretical results are also larger than the available experimental room-temperature thermal conductivity data for cubic-GaP (77 $\mathrm{W\,m^{-1}\,K^{-1}}$ [10] and 100 $\mathrm{W\,m^{-1}\,K^{-1}}$ [11,12]). The substantial difference between the parameters used in different studies in Table I could be the reason for the large difference seen in the corresponding thermal conductivity values. Here, it can also be pointed out that the best agreement with experiment is obtained in an early study [6] employing, by today's standards, a rather small supercell, whereas the worst agreement is found for the largest supercell employed [7] (Table I). It should also be noted that the available experimental data are rather old and not in good internal agreement. A state-of-the-art theoretical prediction could thus be useful, but the poor internal agreement between the theoretical studies means that they contribute little insight into the reliability of the experimental results.

More recently it has become possible to also calculate the scattering due to fourth-order IFCs [13]. Two separate papers [8,9] have demonstrated a substantial reduction of the GaP κ_ℓ due to fourth-order IFCs scattering (Table I). One of these studies [8] agrees well with the low experimental value of 77 $\mathrm{W\,m^{-1}\,K^{-1}}$ whereas the other [9] agrees well with the high experimental value of 100 $\mathrm{W\,m^{-1}\,K^{-1}}$ (Table I).

In the present study we perform *ab initio* calculations to calculate the thermal conductivity of zinc-blende group-III phosphides with special focus on GaP. We elucidate the effect of the aforementioned parameters on the anharmonic IFCs and the thermal conductivity. We explain some of the ambiguity of the earlier literature and find a good agreement between our best possible prediction and the lowest reported experimental thermal conductivity.

II. METHOD

By keeping only the terms linear in ∇T, the lattice thermal conductivity can be expressed as [14]

$$\kappa_\ell^{\alpha\beta} = \frac{k_B}{V_{\mathrm{u.c.}}} \sum_\lambda n_\lambda^0 (n_\lambda^0 + 1) \left(\frac{\hbar\omega_\lambda}{k_B T}\right)^2 v_\lambda^\alpha F_\lambda^\beta, \tag{1}$$

where α and β run over the Cartesian axes, $V_{\mathrm{u.c.}}$ is the unit cell volume, k_B is the Boltzmann constant, and n_λ^0, v_λ^α, and ω_λ are the Bose-Einstein occupancy, the group velocity, and the angular frequency of a phonon mode, respectively. λ is a compound index of the wave vector $\mathbf{q}$ and branch index b. F is given as

$$F_\lambda^\beta = \tau_\lambda^0 \left(v_\lambda^\beta + \Delta_\lambda^\beta\right), \tag{2}$$

where Δ is a linear function of v and $\Delta = 0$ corresponds to the single mode relaxation time approximation that is the

*georg.madsen@tuwien.ac.at

TABLE I. Calculated κ_ℓ for GaP at 300 K together with certain computational parameters from the literature. For the supercell C stands for conventional and P for primitive. For Refs. [8,9] the values obtained including 3ph scattering are listed first, together with those obtained when 4ph scattering was also included.

Study	IFC	Supercell size (atoms)	XC functional	κ_ℓ (W m^{-1} K^{-1})
Lindsay *et al.* [5]	Third	$3\times3\times3$ C (216)	PBE	131
Raya-Moreno *et al.* [7]		$4\times4\times4$ C (512)	LDA	157
Togo *et al.* [6]		$2\times2\times2$ C (64)	LDA	104
Xia *et al.* [8]		$4\times4\times4$ P (128)	PBE	118
Ravichandran *et al.* [9]		$5\times5\times5$ P (250)	LDA	135
Xia *et al.* [8]	Fourth	$4\times4\times4$ P (128)	PBE	84
Ravichandran *et al.* [9]		$5\times5\times5$ P (250)	LDA	107

starting guess for the self-consistent solution of Eq. (1). In the present work, τ_λ^0 is limited by the scattering caused by three-phonon processes and mass disorder due to isotopes by $\tau_\lambda^{\text{iso}}$. Furthermore, scattering due to four-phonon processes is included using a model based on the data available in Ref. [9] as will be discussed below. Three-phonon scattering rates are expressed as [14]

$$\frac{1}{\tau_\lambda^{3\text{ph}}} = \sum_{\lambda'\lambda''}^{+} \Gamma^{+}_{\lambda\lambda'\lambda''} + \sum_{\lambda'\lambda''}^{-} \frac{1}{2}\Gamma^{-}_{\lambda\lambda'\lambda''}. \tag{3}$$

$\Gamma^{+}_{\lambda\lambda'\lambda''}$ and $\Gamma^{-}_{\lambda\lambda'\lambda''}$ denote the scattering rates due to phonon creation and annihilation in three-phonon processes and are given by

$$\Gamma^{+}_{\lambda\lambda'\lambda''} = \frac{\hbar\pi}{4}\frac{n^0_{\lambda'} - n^0_{\lambda''}}{\omega_\lambda\omega_{\lambda'}\omega_{\lambda''}}|V^{+}_{\lambda\lambda'\lambda''}|^2\delta(\omega_\lambda + \omega_{\lambda'} - \omega_{\lambda''}), \tag{4}$$

$$\Gamma^{-}_{\lambda\lambda'\lambda''} = \frac{\hbar\pi}{4}\frac{n^0_{\lambda'} + n^0_{\lambda''} + 1}{\omega_\lambda\omega_{\lambda'}\omega_{\lambda''}}|V^{-}_{\lambda\lambda'\lambda''}|^2\delta(\omega_\lambda - \omega_{\lambda'} - \omega_{\lambda''}), \tag{5}$$

where the scattering matrix elements $V^{\pm}_{\lambda\lambda'\lambda''}$ are

$$V^{\pm}_{\lambda\lambda'\lambda''} = \sum_{i\in\text{u.c.}}\sum_{i',i''}\Phi_{ii'i''}\frac{e_\lambda(i)e_{\pm\lambda'}(i')e_{-\lambda''}(i'')}{\sqrt{M_i M_{i'} M_{i''}}}, \tag{6}$$

$\Phi_{ii'i''}$ is an element of the third-order IFC tensor and the i's the compound indices labeling an atom and a Cartesian direction. M_i is the atomic mass and $e_\lambda(i)$ is the eigenvector of phonon λ projected on the degrees of freedom corresponding to i. The first sum in Eq. (6) runs over the atoms in a reference unit cell, whereas i' and i'' in principle run over all the other atoms in the crystal. In practice the IFCs fall off to zero with distance and the sums are only performed up to a certain cutoff radius. This enters the calculation as a parameter and the larger the supercell, the larger the cutoff radii that can be applied.

III. COMPUTATIONAL DETAILS

All first-principles calculations are done using the VASP code within the projector augmented-wave method [15,16] using a plane-wave cutoff energy of 350 eV and either the local density approximation (LDA) [17,18] or the Perdew-Burke-Ernzerhof (PBE) [19] generalized gradient approximations to the exchange-correlation (XC) functional.

The second- and third-order IFCs are obtained from the forces using the finite-displacement method in $5\times5\times5$ (250 atoms) and $6\times6\times6$ (432 atoms) supercell expansions of the primitive zinc-blende cell using only the Γ point. The set of atomic displacements necessary for extracting the second-order and third-order force constants are obtained using the PHONOPY [20] and SHENGBTE [14] packages, respectively. The third-order IFCs are calculated for atoms within a certain cutoff distance that is systematically increased to include more nearest neighbors (nn) to check for convergence. Two values, 0.01 and 0.03 Å, of the magnitude of finite displacements are chosen to study their effect on the IFCs and κ_ℓ.

The lattice thermal conductivity is calculated using the ALMABTE computer code [21]. A mixed-space approach was used to calculate the nonanalytical term of the dynamical matrix [22]. A sampling mesh of $32\times32\times32$ phonon wave vectors is used.

IV. RESULTS AND DISCUSSION

Table II lists the calculated thermal conductivity for GaP using different computational parameters. First, it is clear that the calculations with 0.01 Å and 0.03 Å finite displacements lead to lattice thermal conductivities that differ substantially. In order to understand this effect better, we study one such triplet interaction, defined by the atoms numbered 0, 1, and 2 in Fig. 1. We displace atoms 1 and 2 in the triplet, and calculate the force on the atom 0. We then calculate the force constant value using the five-point formula

$$\begin{aligned}\Phi^{xxx}_{0,1,2} &= -\left.\frac{\partial^2 f_0^x}{\partial x_1\partial x_2}\right|_{x_1^0,x_2^0}\\ &= \frac{1}{h^2}\left[f_0^x\left(x_1^0+h,x_2^0\right) + f_0^x\left(x_1^0-h,x_2^0\right)\right.\\ &\quad\left. + f_0^x\left(x_1^0,x_2^0+h\right) + f_0^x\left(x_1^0,x_2^0-h\right) - 4f_0^x\left(x_1^0,x_2^0\right)\right],\end{aligned} \tag{7}$$

where f_0^x is the force acting on atom 0 along the x direction, all atomic coordinates other than x_1 and x_2 have been omitted for brevity, and the last term is zero. Figure 1 shows the convergence of $\Phi^{xxx}_{0,1,2}$ with the magnitude of the finite atomic displacements. It reveals two important points. First, in accordance with Table II, we see that for LDA convergence is obtained only after 0.03 Å atomic displacements. Second, in the case of PBE, convergence is much slower and is only obtained only after 0.07 Å. The slow convergence for PBE can be thought of as a consequence of the fact that PBE tends to

TABLE II. Convergence of κ_ℓ at 300 K for GaP with respect to the different calculation parameters for the third-order IFCs. The row labeled LDA (4ph) four-phonon scattering is added as discussed in the main text.

Functional	Displacement (Å)	Supercell size (atoms)	Cutoff up to nn (Å)	κ_ℓ (W m^{-1} K^{-1})
LDA	0.01	5 × 5 × 5 *P* (250)	5 (6.2)	83
	0.03	5 × 5 × 5 *P* (250)	5 (6.2)	122
		6 × 6 × 6 *P* (432)	5 (6.2)	102
		6 × 6 × 6 *P* (432)	6 (6.8)	84
		6 × 6 × 6 *P* (432)	7 (7.3)	85
PBE	0.07	6 × 6 × 6 *P* (432)	6 (7.0)	89
LDA (4ph)	0.03	6 × 6 × 6 *P* (432)	7 (7.3)	76

underbind the atoms leading to smaller forces and therefore larger errors in the force constants.

Table II also documents the dependence of κ_ℓ on the supercell size and the force constant cutoff. Increasing the supercell size from a 250-atom cell to a 432-atom cell decreases the calculated thermal conductivity. This is somewhat surprising considering that the previously largest reported supercell, as seen in Table I, resulted in a large calculated thermal conductivity. However, this calculation also cut the third-order IFCs off at the fourth nearest neighbors. We performed a similar calculation with 0.01 Å finite displacements and a 128-atom supercell where only up to fourth nearest neighbors can be taken into account. Thereby we also obtain a substantially higher thermal conductivity of 153 W m^{-1} K^{-1}, in agreement with Ref. [7]. This would indicate IFCs at larger perimeters that could not be sampled with a fourth-nearest-neighbor cutoff contribute to the scattering. Systematically increasing the cutoff in the 432-atom supercell size up to sixth nearest neighbors we obtain a converged value of 85 W m^{-1} K^{-1} (Table II). This is followed by an equally good agreement between the respective LDA and PBE thermal conductivities, as seen in Table II.

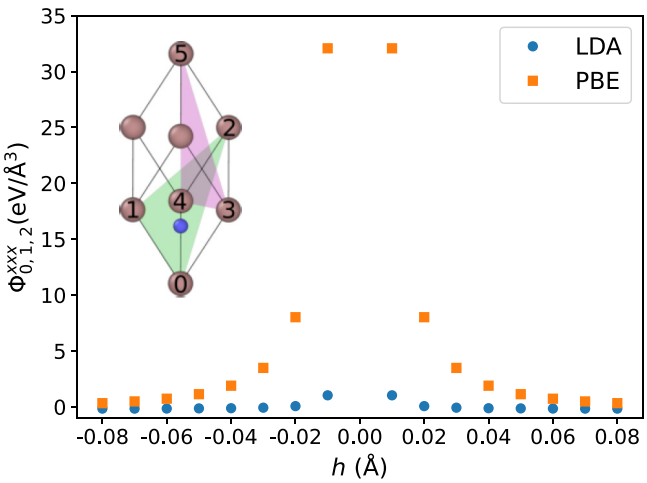

FIG. 1. Convergence of force derivatives, calculated using the standard five-point formula, with respect to the atomic displacement of atoms 1 and 2, in the *x* direction by an amount *h*. The inset shows a primitive cell of GaP with Ga atoms at (0,0,0) positions and P atoms at (1/4, 1/4, 1/4). The green and pink planes show the Ga atom triplets corresponding to the high IFCs seen at perimeters $P \approx 16$ Å and $P \approx 17$ Å in Fig. 2.

The calculated 3ph-limited lattice thermal conductivity at around 85–89 W m^{-1} K^{-1} is in reasonable agreement with the experimental values of 77 W m^{-1} K^{-1} [10] and 100 W m^{-1} K^{-1} [11,12] when considered in the context of the earlier predictions (Table I). However, two earlier studies [8,9] reported a substantial reduction of the calculated thermal conductivity with the inclusion of four-phonon scattering (Table I). These two studies disagree with respect to the magnitude of the predicted lattice thermal conductivity. However, the difference between them can be traced to the 3ph scattering (see Table I), which is understandable considering the present results and the difference in the supercell used in the two studies. In fact, the two studies agree reasonably on the reduction of κ_ℓ due to 4ph scattering being around 30 W m^{-1} K^{-1} (Table I). Reference [9] plots the scattering rates in the Supplemental Material therein where it is seen that the effect of 4ph scattering is limited to a rather narrow frequency range between $f \approx 1.5$ and 3.25 THz, where $\tau^{-1}_{4\text{ph}}$ is comparable to $\tau^{-1}_{3\text{ph}}$. In this region the scattering rates follow a simple exponential trend. Based on the data reported in Ref. [9] we thus introduce a simple model for the 4ph scattering rates given as $\tau^{-1}_{4\text{ph}} = 0.027\ \text{fs}^{-1} \exp(1.84\ \text{THz}^{-1}\, f)$ for the frequency range $f \approx 1.5$–3.25 THz. Adding these scattering rates to $\tau^{-1}_{3\text{ph}}$ and τ^{-1}_{iso} according to Matthiessen's rule reduced the obtained thermal conductivity for the 5 × 5 × 5 supercell from 122 to 105 W m^{-1} K^{-1}. This is in good agreement with the earlier results by Ravichandran [9], who used a similar supercell, thereby validating the procedure. As the 3ph scattering rates are larger using the 6 × 6 × 6 supercell, the effect of the fourth-order scattering is smaller. By including the fourth-order scattering the κ_ℓ is reduced from 85 to 76 W m^{-1} K^{-1}, in very good agreement with the lower experimental value of 77 W m^{-1} K^{-1} at room temperature [10].

The above discussion establishes that the difference in calculated κ_ℓ arises from third-order IFCs that can be included when using large cutoffs. One convenient way of looking for convergence of the third-order IFCs is to plot the norm of the IFC tensor belonging to a particular triplet of atoms versus the perimeter of the triangle formed by that triplet. This is done in Fig. 2 for GaP and shows the presence of high IFCs at large cutoffs. Such high IFCs, seen as purple triangles and red circles at perimeters $P > 16$ Å in Fig. 2, are obtained only when sixth nearest neighbors or more are included in the third-order cutoffs. Those high interactions cannot be sampled

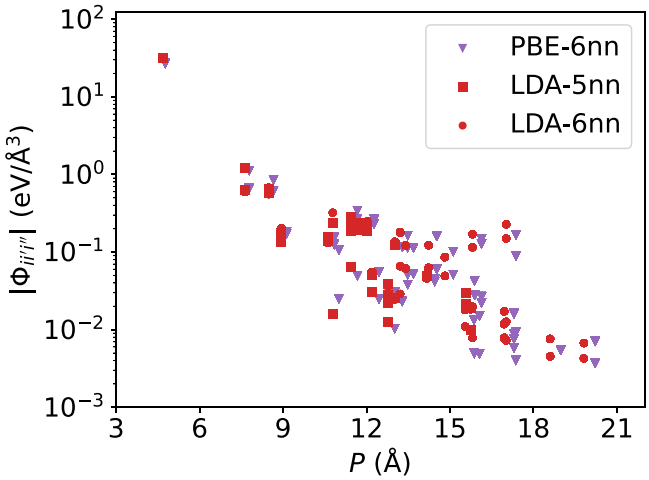

FIG. 2. Convergence for the norm of third-order force constants as a function of triplet triangle perimeter. The force constants have been evaluated for displacements of 0.03 Å (LDA) and 0.07 Å (PBE).

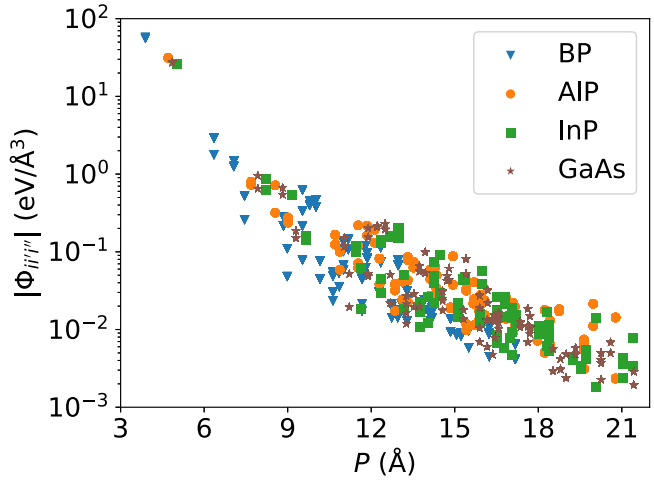

FIG. 4. A comparison of the norm of third-order IFCs convergence when calculated with 0.03 Å finite-displacement values for BP, AlP, InP, and GaAs. All calculation use $6 \times 6 \times 6$ P supercells and seventh-nearest-neighbor cutoffs.

even if we include up to fifth-nearest-neighbor interactions in a $6 \times 6 \times 6$ supercell nor in a $5 \times 5 \times 5$ supercell, which can only account for a maximum of up to fifth-nearest-neighbor interactions. The importance of the long-range third-order IFCs is further illustrated by calculating their contribution [23] to the mode-dependent Grüneisen parameter γ_λ represented in Fig. 3. Similar to an earlier study of Bi and Sb [24], the inclusion of the long-range third-order IFCs show a marked influence on the acoustic bands whereas the opticals are less influenced. The largest influence is found for the longitudinal acoustic band where γ_λ changes substantially for frequencies around 20 rad ps^{-1} underlining the inadequacy of not including the long-range interactions.

For the third-order IFCs of the other group-III phosphides a smooth convergence is observed with a cutoff distance (Fig. 4) and the high interactions at larger atomic distances found in GaP are absent. As a result the thermal conductivity values

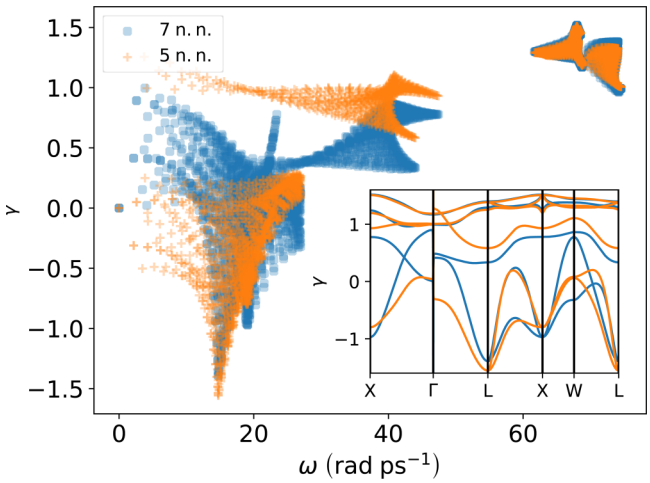

FIG. 3. Calculated Grüneisen parameter using two different third-order cutoffs. The large plot is a scatter plot of all bands on a regular mesh throughout the Brillouin zone and the inset shows specific directions.

for group-III phosphides (Table III) show no drastic differences when including higher third-order IFC cutoffs in the calculation of the scattering matrix elements [Eq. (6)]. This is in agreement with the literature values for κ_ℓ of the other group-III phosphides being much less spread out.

That the phosphides listed in Table III do not show an unusual dependence of the calculated thermal conductivity on the cutoff distance is in accordance with the earlier observation of the role of long-range Ga-Ga-Ga interactions in determining the thermal conductivity of GaP (Fig. 2). In order to understand whether these interactions are somehow intrinsic to the Ga sublattice, we studied the effect of the cutoff distance and finite-displacement distance on the third-order IFCs and κ_ℓ of GaAs. Again, a smooth convergence of the third-order IFCs is found (Fig. 4), suggesting that the presence of strong interactions at larger atomic distances in GaP are indeed specific to the GaP system. Furthermore, we find a calculated GaAs thermal conductivity (≈45 W m^{-1} K^{-1}), in good agreement with recent experimental [25,26] and theoretical values [7,27,28], that is converged already for the $5 \times 5 \times 5$ supercell as no further large IFCs are obtained for the bigger supercell. While the long-range Ga-Ga-Ga interactions do seem to be a peculiarity of GaP, it should be pointed

TABLE III. Convergence of room-temperature κ_ℓ with respect to the different calculation parameters for the third-order IFCs in group-III phosphides. All the calculations are done in $6 \times 6 \times 6$ supercells containing 432 atoms each with displacements of 0.03 Å.

Compound	Cutoff up to nn	κ_ℓ (W m^{-1} K^{-1})
BP	5	463
	7	470
AlP	5	97
	7	85
InP	5	96
	7	91

out that similar long-range interactions have previously been found to be decisive for the thermal conductivity in number of compounds containing heavy elements [24,29].

V. CONCLUSIONS

In this study we calculated the lattice thermal conductivity of the group-III phosphides. We have shown how the convergence with respect to the underlying parameters such as the supercell size, the magnitude of the finite atomic displacements, and the cutoff for the third-order atomic interactions, plays a vital role in calculating the thermal conductivity of cubic GaP. We explain some of the ambiguity of the earlier literature on GaP and show how the presence of high IFCs at large perimeters on the Ga sublattice need to be accounted for using a large supercell with up to sixth-nearest-neighbor interactions. When both 4ph scattering and the contributions from long-range interactions are included in the calculation of 3ph scattering, a thermal conductivity of 76 $\mathrm{W\,m^{-1}\,K^{-1}}$ is obtained at room temperature, in good agreement with a reported experimental value of 77 $\mathrm{W\,m^{-1}\,K^{-1}}$. We found these interactions to be specific to the GaP system. Our study shows that it is imperative to pay close attention to all the associated parameters for the *ab initio* thermal conductivity calculations and could serve as a guide for other systems where such high IFC patterns exist.

ACKNOWLEDGMENTS

We thank Martí Raya-Moreno for pointing out Refs. [24,29] and the Austrian Science Funds (FWF) for funding under project CODIS (Grant No. FWF-I-3576-N36).

[1] S. Ehsanfar, F. Kanjouri, H. Tashakori, and A. Esmailian, First-principles study of structural, electronic, mechanical, thermal, and phonon properties of III-phosphides (BP, AlP, GaP, and InP), J. Electron. Mater. **46**, 6214 (2017).

[2] J. Miao, C. Chai, W. Zhang, Y. Song, and Y. Yang, First-principles study on structural, mechanical, anisotropic, electronic and thermal properties of III-phosphides: XP (X = Al, Ga, or In) in the P6422 phase, Materials **13**, 686 (2020).

[3] D. A. Broido, M. Malorny, G. Birner, N. Mingo, and D. A. Stewart, Intrinsic lattice thermal conductivity of semiconductors from first principles, Appl. Phys. Lett. **91**, 231922 (2007).

[4] A. J. H. McGaughey, A. Jain, H.-Y. Kim, and B. Fu, Phonon properties and thermal conductivity from first principles, lattice dynamics, and the Boltzmann transport equation, J. Appl. Phys. **125**, 011101 (2019).

[5] L. Lindsay, D. A. Broido, and T. L. Reinecke, *Ab initio* thermal transport in compound semiconductors, Phys. Rev. B **87**, 165201 (2013).

[6] A. Togo, L. Chaput, and I. Tanaka, Distributions of phonon lifetimes in Brillouin zones, Phys. Rev. B **91**, 094306 (2015).

[7] M. Raya-Moreno, R. Rurali, and X. Cartoixà, Thermal conductivity for III-V and II-VI semiconductor wurtzite and zinc-blende polytypes: The role of anharmonicity and phase space, Phys. Rev. Mater. **3**, 084607 (2019).

[8] Y. Xia, V. I. Hegde, K. Pal, X. Hua, D. Gaines, S. Patel, J. He, M. Aykol, and C. Wolverton, High-Throughput Study of Lattice Thermal Conductivity in Binary Rocksalt and Zinc Blende Compounds Including Higher-Order Anharmonicity, Phys. Rev. X **10**, 041029 (2020).

[9] N. K. Ravichandran and D. Broido, Phonon-Phonon Interactions in Strongly Bonded Solids: Selection Rules and Higher-Order Processes, Phys. Rev. X **10**, 021063 (2020).

[10] E. F. Steigmeier and I. Kudman, Acoustical-optical phonon scattering in Ge, Si, and III-V compounds, Phys. Rev. **141**, 767 (1966).

[11] H. Weiß, Thermospannung und Wärmeleitung von III-V-Verbindungen und ihren Mischkristallen, Ann. Phys. **459**, 121 (1959).

[12] H. Wagini, Die Wärmeleitfähigkeit von GaP und AlSb, Z. Naturforsch. A **21**, 2096 (1966).

[13] T. Feng and X. Ruan, Quantum mechanical prediction of four-phonon scattering rates and reduced thermal conductivity of solids, Phys. Rev. B **93**, 045202 (2016).

[14] W. Li, J. Carrete, N. A. Katcho, and N. Mingo, ShengBTE: A solver of the Boltzmann transport equation for phonons, Comput. Phys. Commun. **185**, 1747 (2014).

[15] G. Kresse and J. Furthmüller, Efficient iterative schemes for *ab initio* total-energy calculations using a plane-wave basis set, Phys. Rev. B **54**, 11169 (1996).

[16] G. Kresse and D. Joubert, From ultrasoft pseudopotentials to the projector augmented-wave method, Phys. Rev. B **59**, 1758 (1999).

[17] W. Kohn and L. J. Sham, Self-consistent equations including exchange and correlation effects, Phys. Rev. **140**, A1133 (1965).

[18] J. P. Perdew and A. Zunger, Self-interaction correction to density-functional approximations for many-electron systems, Phys. Rev. B **23**, 5048 (1981).

[19] J. P. Perdew, K. Burke, and M. Ernzerhof, Generalized Gradient Approximation Made Simple, Phys. Rev. Lett. **77**, 3865 (1996).

[20] A. Togo and I. Tanaka, First principles phonon calculations in materials science, Scr. Mater. **108**, 1 (2015).

[21] J. Carrete, B. Vermeersch, A. Katre, A. van Roekeghem, T. Wang, G. K. H. Madsen, and N. Mingo, almaBTE : A solver of the space-time dependent Boltzmann transport equation for phonons in structured materials, Comput. Phys. Commun. **220**, 351 (2017).

[22] Y. Wang, J. J. Wang, W. Y. Wang, Z. G. Mei, S. L. Shang, L. Q. Chen, and Z. K. Liu, A mixed-space approach to first-principles calculations of phonon frequencies for polar materials, J. Phys.: Condens. Matter **22**, 202201 (2010).

[23] D. A. Broido, A. Ward, and N. Mingo, Lattice thermal conductivity of silicon from empirical interatomic potentials, Phys. Rev. B **72**, 014308 (2005).

[24] S. Lee, K. Esfarjani, J. Mendoza, M. S. Dresselhaus, and G. Chen, Lattice thermal conductivity of Bi, Sb, and Bi-Sb alloy from first principles, Phys. Rev. B **89**, 085206 (2014).

[25] M. G. Holland, Phonon scattering in semiconductors from thermal conductivity studies, Phys. Rev. **134**, A471 (1964).

[26] A. V. Inyushkin, A. N. Taldenkov, A. Y. Yakubovsky, A. V. Markov, L. Moreno-Garsia, and B. N. Sharonov, Thermal conductivity of isotopically enriched ^{71}GaAs crystal, Semicond. Sci. Technol. **18**, 685 (2003).

[27] T. Luo, J. Garg, J. Shiomi, K. Esfarjani, and G. Chen, Gallium arsenide thermal conductivity and optical phonon relaxation times from first-principles calculations, Europhys. Lett. **101**, 16001 (2013).

[28] M. Arrigoni, J. Carrete, N. Mingo, and G. K. H. Madsen, First-principles quantitative prediction of the lattice thermal conductivity in random semiconductor alloys: The role of force-constant disorder, Phys. Rev. B **98**, 115205 (2018).

[29] S. Lee, K. Esfarjani, T. Luo, J. Zhou, Z. Tian, and G. Chen, Resonant bonding leads to low lattice thermal conductivity, Nat. Commun. **5**, 3525 (2014).